Human Molecular Genetics, 2018, Vol. 27, No. 19 3377–3391

doi: 10.1093/hmg/ddy246
Advance Access Publication Date: 8 August 2018
General Article

GENERAL ARTICLE

Mutation of FOP/FGFR1OP in mice recapitulates human short rib-polydactyly ciliopathy

Olivier Cabaud, Régine Roubin, Audrey Comte, Virginie Bascunana, Arnauld Sergé, Fatima Sedjaï, Daniel Birnbaum, Olivier Rosnet† and Claire Acquaviva*

Aix-Marseille Univ, Inserm, CNRS, Institut Paoli-Calmettes, CRCM, Marseille, France

*To whom correspondence should be addressed at: 27 Bd Lei Roure, BP30059, 13273 Marseille Cedex09, France. Tel: +33 486 977 262; Fax: +33 486 977 499; Email: claire.acquaviva@inserm.fr

Abstract

Skeletal dysplasias are a clinically and genetically heterogeneous group of bone and cartilage disorders. A total of 436 skeletal dysplasias are listed in the 2015 revised version of the nosology and classification of genetic skeletal disorders, of which nearly 20% are still genetically and molecularly uncharacterized. We report the clinical and molecular characterization of a lethal skeletal dysplasia of the short-rib group caused by mutation of the mouse *Fop* gene. *Fop* encodes a centrosomal and centriolar satellite (CS) protein. We show that *Fop* mutation perturbs ciliogenesis *in vivo* and that this leads to the alteration of the Hedgehog signaling pathway. *Fop* mutation reduces CSs movements and affects pericentriolar material composition, which probably participates to the ciliogenesis defect. This study highlights the role of a centrosome and CSs protein producing phenotypes in mice that recapitulate a short rib-polydactyly syndrome when mutated.

Introduction

Most vertebrate cells have surface hair-like projections called cilia. Single non-motile cilia, called primary cilia (PC), are found at the surface of almost all cell types. Multiple motile cilia, found on specialized epithelia such as the oviduct and the respiratory tract, produce directional fluid flows. PC are antenna-like cellular organelles that act as sensors and play an important role in signal transduction (1–3). All cilia are microtubule (MT)-based structures formed by a core axoneme that nucleates from centrosome-related structures. A single centrosome can generate a unique basal body from its mother centriole that will dock at the cell membrane and act as a template for the axoneme that assembles a cilium (4,5). Alternatively, multiciliated cells can generate hundreds of basal bodies and cilia through a specific mode of centriole amplification via deuterosomes (4,6). In cycling cells PC formation and disassembly is dependent upon various factors and regulated during the cell cycle to allow centrosomal spindle assembly in mitosis (7–9).

Although the mechanisms are still not completely understood (for a recent review see 10), cilia assembly and maintenance universally relies on a selective transport system for ciliary proteins, called intraflagellar transport (IFT) (11,12). IFT relies on large multiprotein complexes that use molecular motors to carry architectural (such as tubulin), or signaling components (such as receptors), in or out of the cilium to maintain the appropriate supply for cilia composition and function. Traffic in and out of the cilia is also controlled by the transition zone, distal to the basal body, which acts as a ciliary gate (13). The Bardet-Biedl syndrom (BBS)ome

†Present address : Institut de Biologie du Développement de Marseille, Aix-Marseille-Université, CNRS 7288, F-13009 Marseille, France.
Received: February 26, 2018. **Revised:** June 28, 2018. **Accepted:** June 29, 2018

complex also regulates ciliary trafficking of several signaling molecules. The BBSome is indispensable for ciliogenesis and transportation within cilia. It is required for IFT assembly at the basal body, IFT transport and IFT recycling (14,15). It constitutes a coat complex that sorts membrane proteins to PC (16) and participates in ciliary membrane extension by activation of RAB8 (17). CSs are also involved in ciliary construction, maintenance and function by regulating the recruitment of proteins (like BBSome proteins) to the basal body and cilium (18–20). CSs may act as assembly or reservoir points for centriole and basal body proteins (21). CSs are electron dense, non-membranous 70 to 100 nm cytoplasmic granules formed by multiprotein complexes. They concentrate around the centrosomes and basal bodies in animal cells. They are composed of more than 30 proteins. They are dynamic structures trafficking along MTs towards and away from the centrosome using dynein and kinesin motors. CSs are also potential regulators of centriole duplication (22,23). CSs are defined by pericentriolar material (PCM) 1 (PCM1), their key scaffolding component (20,24). The deletion of the gene encoding the PCM1 protein induces the loss of satellites and a major defect in ciliogenesis (20). CSs have multiple roles in cell biology on top of their role in ciliogenesis, from neurogenesis to genomic stability or adaptation to stress (18,25–27). Different categories of CSs exist according to their composition. CSs are essential actors in centrosome and PCM composition. Although the proteome of CSs is only partially known (28), a number of proteins are associated with them, several of which are mutated in patients with ciliopathies. Indeed, CSs are involved in the ciliary targeting of OFD1 and CEP290, e.g. (29,30). However, the functional significance of CSs in mammalian development and ciliogenesis *in vivo* remains unclear.

Cilia regulate development through a number of signaling pathways such as platelet-derived growth factor receptor (PDGFR), WNT or Hedgehog, and the alteration of cilia structure and function can cause a wild spectrum of developmental diseases called ciliopathies (31–35). Among them are skeletal dysplasia called the short rib-polydactyly syndromes (SRPSs) (36). This group of disorders is characterized by skeletal defects, short ribs and limbs, and polydactyly. SRPSs include four lethal conditions: Verma-Naumoff syndrome (SRP type III), Majewski syndrome (SRP type II), Saldino-Noonan syndrome (SRP type I) and Beemer-Lamger syndrome (SRP type IV), and four conditions compatible with life: Jeune syndrome or asphyxiating thoracic dysplacia (ATD), Ellis-van Creveld syndrome (EVC), Sensenbrenner syndrome and Weyers acrofacial dysostosis. Mutations causative of SRPSs have been found in *IFT* genes (with mutations found in the following 10 *IFT* genes: *IFT122, 140, 172, 43, 80, 144* and *WDR19, 34, 35, 60*), in the motor *DYNC2H1* gene, in one transition zone coding gene (*TCTN3*) and in seven centrosome/basal body function-related genes (*CSPP1, NEK1, NEK9, EVC* and *EVC2, CCCDC100/CEP120* and *Talpid3/KIAA0586*). In a number of cases the genetic cause is however still unknown. SRPSs are rare and often embryonic lethal conditions, which complicates the physiopathology analysis of the disease.

We report here a mouse model of SRPS caused by the mutation of the centrosomal and CS protein FOP. This protein was initially identified in our laboratory in a myeloproliferative syndrome (37,38). We have shown that it is involved in cell cycle regulation and cell survival (39). Moreover, it was shown to participate in a complex necessary for MT anchoring to the centrosome (40) and in ciliogenesis (41,42). In addition to *in vitro* identification of genes and proteins involved in the formation and function of centrosome/cilium, there is a need to study these putative human disease genes during development and disease.

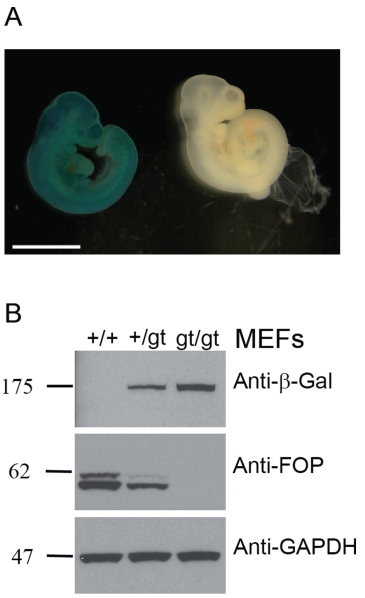

Figure 1. Mouse gene trap characterization. **(A)** Whole mount β-Gal staining of $Fop^{+/+}$ and $Fop^{+/gt}$ 10.5 dpc mouse embryos. Scale bar represents 2 mm. **(B)** Western blot of cell extracts from $Fop^{+/+}$, $Fop^{+/gt}$ or $Fop^{gt/gt}$ MEFs. The same membrane was probed with anti-β-Gal (detects the gene trap protein product), anti-FOP (detects FOP wild-type protein), anti-GAPDH antibodies (as loading control).

To have a better understanding of FOP function, we studied FOP *in vivo* in a model organism. We have generated a transgenic mouse model in which a gene trap creates a mutation in the *Fop* gene. We have found that *Fop* mutation reproduces in the animal the characteristics of a human SRPS with narrow chests, short limbs and polydactyly. *Fop* mutation perturbs ciliogenesis *in vivo* and this leads to the alteration of the Hedgehog signaling pathway. It also reduces CSs movements and affects PCM composition, which shows a possible molecular mechanism for FOP involvement in ciliogenesis.

Results

$Fop^{gt/gt}$ mouse generation and characterization

To study the function of FOP *in vivo* we created a mutant mouse using embryonic stem cells (ES cells) in which the *Fop* sequence is interrupted by the insertion of a gene trap cassette in the intronic region downstream of exon 5 (Supplemental Fig. S1A). The functionality of the gene trap was assayed by reverse transcriptase-polymerase chain reaction (RT-PCR) to detect either the wild-type transcript or a chimeric transcript composed of the *Fop* first 5 exons followed by a β-*Geo* sequence (Supplemental Fig. S1B). The gene trap allele will be referred to as Fop^{gt}. We confirmed the gene trap insertion by Northern blotting (Supplemental Fig. S1C). Our studies were conducted in the mixed C57BL/6 x 129 genetic background (designated B6;129), and we also backcrossed $Fop^{+/gt}$ mice to obtain C57BL/6 and BALB/c pure backgrounds.

Expression of β-Gal from the $Fop^{gt/gt}$ alleles was assessed in whole-mount embryos. At the earliest time tested (10 dpc, Fig. 1A) and later developmental stages (14.5 dpc, Supplemental Fig. S1D) the expression was ubiquitous although stronger in some tissues. The expressed protein concentrated in restricted areas in the cell at the apical side of polarized epithelia, suggesting a localization of the gene product at basal bodies of multiciliated cells (Supplemental Fig. S1E).

In protein extracts obtained from mouse embryonic fibroblasts (MEFs) derived from the three genotypes, we confirmed the expression of a chimeric protein composed of FOP N-terminus fused to the β-Geo reporter (Fig. 1B).

Fop mutation results in embryonic lethality and developmental anomalies

At birth, heterozygous *Fop*$^{+/gt}$ animals had no discernable phenotype and thrived normally. They later developed obesity independently of the sex and genetic background (Supplemental Fig. S2A, B and C). We never obtained homozygous pups (*Fop* $^{gt/gt}$) and the genotype ratios at birth were 37% of *Fop*$^{+/+}$ (n = 276) and 63% *Fop*$^{+/gt}$ (n = 474). Homozygous mutation of *Fop* thus led to embryonic lethality, indicating an essential role for FOP in normal embryonic development. Lower than expected Mendelian ratio of homozygotes at 8.5 dpc indicated early lethality. For most embryos surviving the first week of gestation lethality occurred perinatally (Fig. 2A).

We analyzed homozygous embryos to determine the developmental defects caused by the *Fop* mutation. In the three genetic backgrounds, 93% of *Fop*$^{gt/gt}$ embryos were smaller than their wild-type or heterozygous littermates (Fig. 2B and G) (n = 46), indicating a growth defect. They very frequently presented skeletal dysmorphia. The most obvious phenotype was polydactyly, with 89% of embryos presenting finger number abnormality (on the forelimb and/or hindlimb) (Fig. 2C and Supplementary Fig. S3A) (n = 35). In skeletal stainings embryos also showed a shortening and bowing of long bones (Fig. 2B and C,Supplementary Fig. S3A and data not shown for BALB/c), constricted thoracic cages and irregular ribs with occasional fusion or forking, misaligned and incomplete sternal vertebrae (Fig. 2D and Supplementary Fig. S3B), reduced or absent ossification of the vertebral bodies of the cervical and thoracic vertebrae (Fig. 2E) and facial malformation with hypomineralized skull (Fig. 2B). Embryos of both backgrounds also showed occasional absence of abdominal wall closure (42%, n = 38) and oedemas in various locations (38%, n = 26) (Fig. 2F). We looked in B6;129 and C57BL/6 embryos and observed ventricular heart hypoplasia and hypoplastic lungs, with an absence of expanded saccules as if the embryonic lung development had been arrested before the terminal stage, i.e. the saccular stage (Fig. 2G and H). These alterations probably explain why homozygotes died perinatally. Altogether, these phenotypes are reminiscent of the group of diseases called ciliopathies, and more specifically of SRPSs. SRPSs regroup skeletal dysplasias including four perinatal lethal conditions (SRPS types I–IV) and two other similar skeletal disorders, EVC syndrome and ATD.

Developmental anomalies in FOP mutants are associated with defects in ciliogenesis and impaired Hedgehog signaling

SRPSs, and more generally ciliopathies, are due to the mutation of genes associated with cilia structure or function. This prompted us to examine whether *Fop* mutation caused a defect in the capacity of cells to grow cilia.

We looked whether ciliogenesis was affected *in vivo*. We analyzed embryonic kidneys of *Fop*$^{gt/gt}$ embryos and observed that cilia were absent in most renal tubules (six kidneys analyzed), in contrast with renal tubules from *Fop*$^{+/+}$ mice (seven kidneys analyzed) (Fig. 3A). Centrosomes/basal bodies were, however, correctly positioned at the apical plasma membrane. We also looked at embryonic lungs (Fig. 3B) and observed a reduction of multiciliated cells in the airway epithelium, which was variable between samples (n = 3). In both kidneys and lungs we observed a stronger accumulation of acetylated tubulin inside the cells that do not present cilia at their surface. To have a more general view of tissues in which *Fop* mutation may impact ciliogenesis, we analyzed sagittal sections of full-size wild-type embryos at 15.5 or 16.5 dpc. We observed that a large majority of tissue present PC at this stage of embryonic development. We noticed that PC were also easily detected at the same positions in mutant embryos. This is illustrated in Fig. 3C with PC detection in primordia of follicles of vibrissae associated with the upper lip. In conclusion, *Fop* mutation inhibits ciliogenesis, but this does not extend to every embryonic tissue.

While this work was in progress the inhibition of FOP expression by small interfering RNA (siRNA) in hTert-RPE1 cells was shown to inhibit ciliogenesis (41). We did the same observation in this cell line (data not shown). To further analyze the specific effect of the *Fop* mutation we derived MEFs from *Fop*$^{+/+}$ and *Fop*$^{gt/gt}$ embryos. MEFs from the two genotypes had similar proliferative capacities. The distribution between the different phases of the cell cycle (G1/S/G2-M) and the proliferative index determined by KI67 positive staining was similar for *Fop*$^{+/+}$ and *Fop*$^{gt/gt}$ cells (Fig. S4A). In a previous work we analyzed the effect of the complete deletion of FOP expression *in vitro* and observed cell cycle progression defects with cells arresting in G1 before dying (39). This was not the case here, which indicates that the gene trap mutant conserves some function(s) necessary for cell cycle progression. We next analyzed the capacity of the derived fibroblasts to grow PC in culture. Cilia formation is favored when cells exit the cell cycle, for instance when serum starved. Starved mutant cells exited the cell cycle as well as wild-type cells (as checked by flow cytometry with an anti-KI67 staining, Fig. S4B) but 39% of *Fop*$^{+/+}$ cells presented a cilium versus 14% of *Fop*$^{gt/gt}$ cells. Moreover, in ciliated *Fop*$^{gt/gt}$ cells, the cilium was shorter than in *Fop*$^{+/+}$ cells (Fig. 4A). This was checked with different cilia markers: two modified forms of α-Tubulin (acetylated tubulin and detyrosinated tubulin) and the small G protein ARL13B. Ciliogenesis was rescued in *Fop*$^{gt/gt}$ cells to control level by the transfection of a Myc-tagged construct of wild-type *Fop*; both the number of ciliated cells and cilia length reverted to wild-type values in transfected cells (Fig. 4A, Supplementary Fig. S5). *Fop*$^{gt/gt}$ cells express a mutated version of FOP composed of the N-terminal part of FOP fused to β-Geo (Supplementary Fig. S1A). We wanted to know if the defect in ciliogenesis was due to the absence of the C-terminal part of the protein and/or the fusion with the protein β-Geo. We tested the rescue of ciliogenesis in *Fop*$^{gt/gt}$ with a construct called FOP Δ-Cter, composed of the part of FOP conserved in the gene trap mutant. This construct could be detected specifically with a Myc tag. It localized like the wild-type protein at the centrosomes and CSs. If the defect in ciliogenesis was due to the absence of the C-terminal part of the protein, the expression of FOP Δ-Cter should not rescue the phenotype. We observed that this construct was able to restore ciliogenesis (Fig. 4A). This indicated that the fusion with β-Geo, instead of the C-terminal part of the protein, is responsible for the defect in ciliogenesis, probably perturbing FOP's interactions with partners. The FOP Δ-Cter construct was less efficient than the full-length FOP to permit ciliogenesis. This indicated that the C-terminal part of the protein participates also in FOP function in ciliogenesis. However, we did not try to rescue the mutant phenotype with the C-terminal part of FOP because it was shown not to localize properly (40).

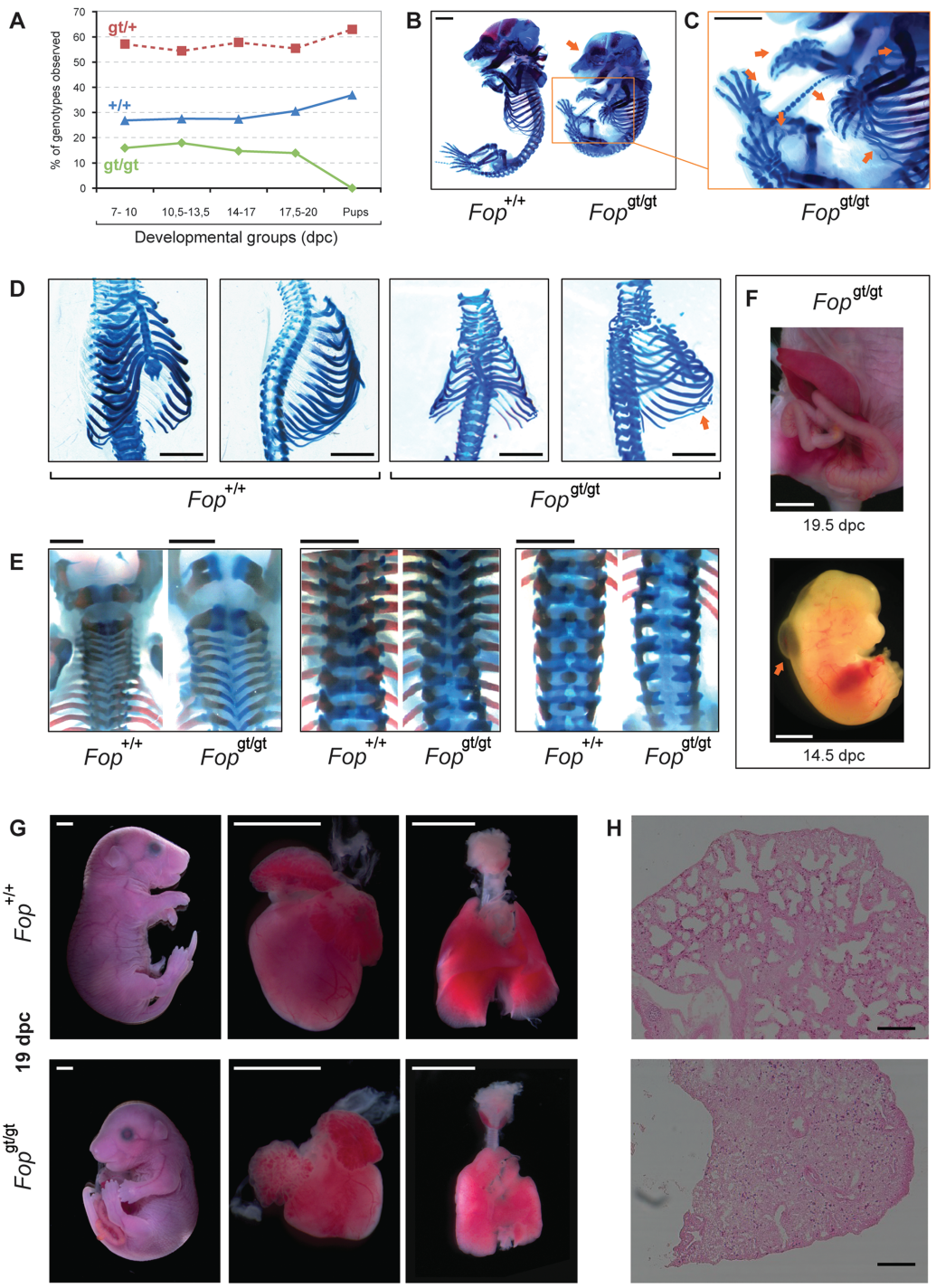

Figure 2. Homozygous mutant embryos present various defects such as a smaller size and skeletal anomalies reminiscent of SRPS. **(A)** Graphic representation of the ratio of $Fop^{+/+}$, $Fop^{+/gt}$ and $Fop^{gt/gt}$ pups in litters according to gestational ages. A minimum of 18 litters was analyzed for each developmental range (8.5–10, 10.5–13.5, 14–17, 17.5–20 dpc, pups). This indicates that about one-third of $Fop^{gt/gt}$ embryo die before 8.5 dpc and the rest die perinatally. **(B)** General view of alcian blue (cartilage) and alizarin red (bone) staining of 19.5 dpc embryos. Mutant embryos are smaller than wild-type littermates. Arrows indicate skeletal anomalies (hypomineralized skull, polydactyly, short and bowed long bone and forking rib). Scale bar represents 2 mm. **(C)** is a magnified view of the squared area in (B). Scale bar represents 2 mm. **(D)** Rib cages from homozygous mutant are smaller and irregular. Ribs can be bifide (arrow) or fused together. Scale bar represents 2 mm. **(E)** Absence of fusion and misalignment of the cervical vertebrae (left panel) is observed in $Fop^{gt/gt}$ embryos. Dorsal view of the thoracic (middle panel) and lumbar (right panel) vertebrae shows reduced or absent ossification of the vertebral bodies as well as reduced laminae in $Fop^{gt/gt}$ compare to $Fop^{+/+}$ embryos. Scale bars represent 1 mm. **(F)** Examples of abdominal wall closure defect in a 19.5 dpc homozygous embryo (top) and oedema (indicated by an arrow) in a 14.5 dpc homozygous embryo (bottom). Scale bar represents 2 mm. **(G)** Mutant embryos are smaller than wild-type littermates and have heart and lung hypoplasia. Scale bar represents 2 mm. **(H)** Lung sections H&E stained show abnormal alveolar development. Scale bar represents 400 µm.

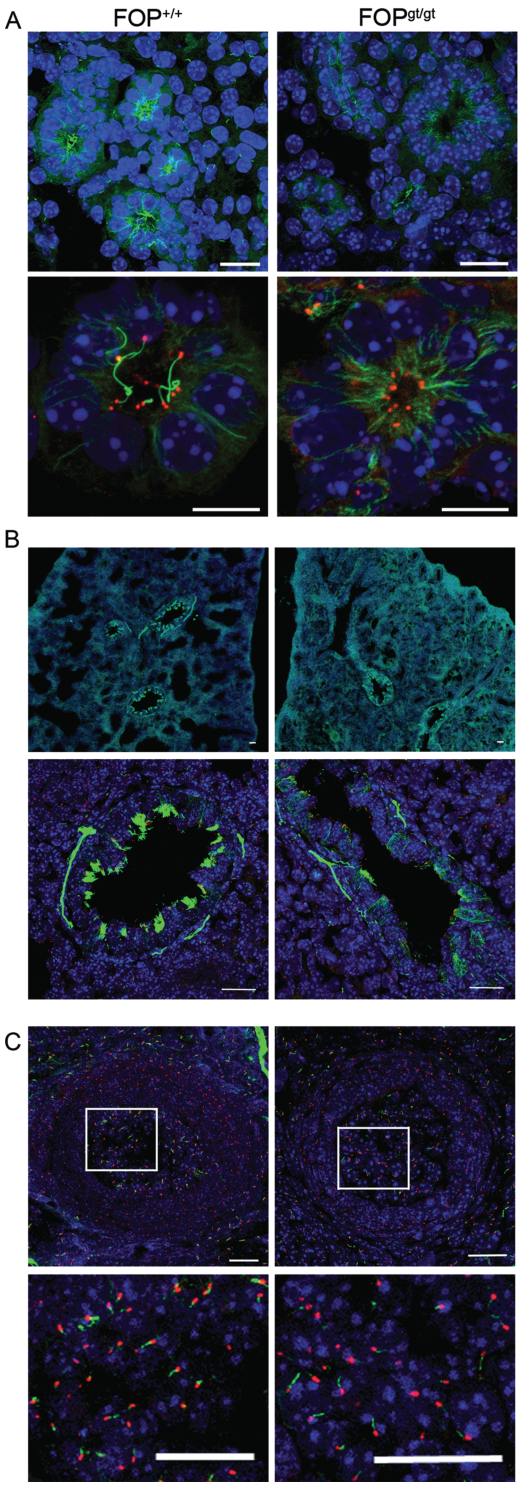

Figure 3. *In vivo* ciliogenesis alteration. Immunofluorescence of **(A)** embryonic kidney sections (E17.5 dpc), **(B)** embryonic lungs (E17.5 dpc) of *Fop*$^{+/+}$ or *Fop* $^{gt/gt}$ mouse embryos staining the primary cilia (green, anti-acetylated tubulin) and nuclei (blue) on the top row (scale bar represents 20 µm). Larger magnification of the sections are represented in the bottom row and were stained to detect the primary cilia (green, anti-acetylated tubulin), FOP (red) and DNA (blue, DAPI). Scale bar represents 20 µm. **(C)** Immunofluorescence of primordial follicles of vibrissae in sagittal sections of *Fop*$^{+/+}$ or *Fop*$^{gt/gt}$ mouse embryos at E16.5 dpc staining the primary cilia (green, anti-acetylated tubulin), FOP (red) and nuclei (blue) on the top row (scale bar represents 20 µm). Larger magnifications of the sections are represented in the bottom row (scale bar represents 20 µm).

Given the role of the PC in signal transduction and the important role of the Hedgehog pathway in skeletal development (43,44) we examined whether the activation of this pathway was altered in FOP mutant cells. We stimulated MEFs derived from *Fop*$^{gt/gt}$ or *Fop*$^{+/+}$ embryos with an Sonic hedgehog (SHH) agonist and measured the induction of *Ptch1* and *Gli1*, two SHH-responsive mRNAs, by quantitative RT-PCR (Fig. 4B). FOP mutation drastically impaired SHH target genes induction upon stimulation with an agonist for 24 or 48 h. Smoothened (SMO) enrichment in cilia is critical for the activation of the hedgehog (HH) pathway. Thus, we analyzed if SMO relocalization to the cilia was still possible in the small percentage of *Fop*$^{gt/gt}$ cells mutant cells that still present a cilia, although shorter than in the wild-type situation (Fig. 4A). By immunofluorescence we observed that SMO correctly localizes in the remaining cilia (Fig. 4C). This suggests that, when FOP is mutated, ciliation is much less efficient, but when cilia are built, they respond to HH induction. The lack of HH signal transduction is thus probably due to the poorly efficient ciliation.

FOP mutation affects PCM1 satellites function and PCM composition

To understand how FOP participates in ciliogenesis we analyzed the localization of the mutant FOP. Immunofluorescences with anti-FOP and anti-β-Gal antibodies permitted the localization of the chimeric protein and gave signals that perfectly co-localized. The chimeric protein localized, like the wild-type protein, at the centrosome (identified by C-NAP1/CEP250 staining) and at the CSs (identified by PCM1 staining) (Fig. 5A). When we compared centrosomes and CSs in *Fop*$^{+/+}$ and *Fop*$^{gt/gt}$ MEFs we observed that some dots were larger than regular satellites in *Fop*$^{gt/gt}$ MEFs. Some of these FOP accumulation spots were negative for C-NAP1 or Centrin staining (Fig. 5A and Supplementary Fig. S6A and thus did not correspond to supernumerary centrosomes. Instead, they were positive for PCM1 staining, the typical marker of CSs (Fig. 5A). In control cells, CSs were distributed as a gradient of granules centered on the centrosome. In mutant cells we observed a heterogeneity in the size of the satellites and their distribution was more random and rarely in a concentric gradient around the centrosome. Satellites can bring cargos to the centrosome or sequester proteins away from it and control centrosomal and PCM protein composition (19–21). We checked Pericentrin and γ-Tubulin concentration in the PCM and noticed increased levels in mutant cells (Fig. 5B). In conclusion, CS intracellular distribution, CS and PCM composition were altered in mutant cells compared to control cells.

Satellites are dynamic particles moving along MTs. We wished to understand why CS dynamics resulted in this aberrant intracellular distribution and perturbed PCM composition. To follow CS behavior we chose to visualize PCM1 coupled to green fluorescent protein (GFP). We observed that overexpression of PCM1 led to protein aggregates in the cytoplasm. To be closer to physiological levels of the protein we used HeLa-Kyoto cells (TransgeneOmics cells, 45) expressing PCM1 fused to GFP from bacterial artificial chromosome (BAC) transgenes, which ensures the presence of most, if not all, regulatory elements (45). We selected a clone that expresses enough GFP-PCM1 to be followed in live cell microscopy, but with no increase in the global (endogenous and GFP-labelled) PCM1 protein level compared to the control cell line as detected by Western blotting (Fig. S6B). In this clone we did not observe an alteration of PCM1 satellite distribution, and noticed that we could detect

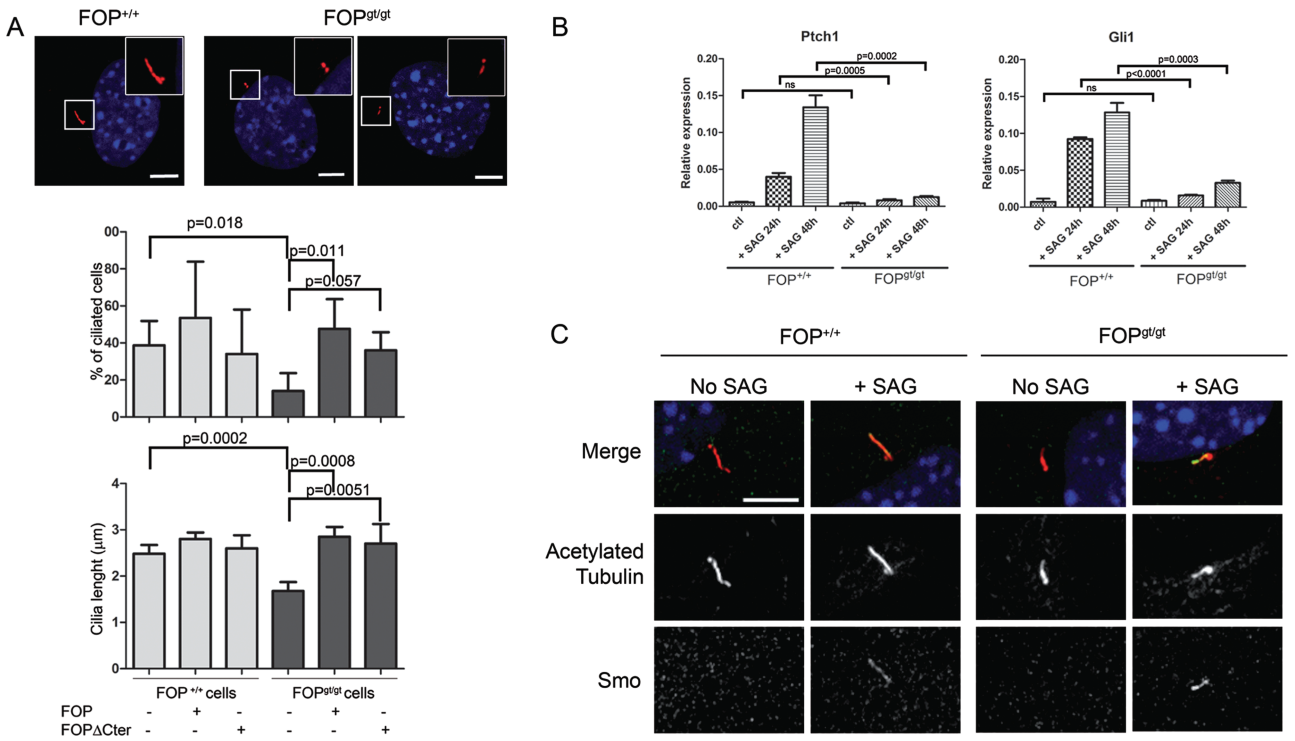

Figure 4. *In vitro* ciliogenesis alteration and defective Hedgehog signaling. **(A)** Representative immunofluorescence of *Fop*$^{+/+}$ or *Fop*$^{gt/gt}$ MEFs serum starved to induce ciliation and stained with anti-acetylated tubulin antibodies to detect the primary cilia (red). The left picture is a representative image of a cilia in *Fop*$^{+/+}$cells (present on 39% of the cells) and right pictures are representatives images of *Fop*$^{gt/gt}$ presenting no cilia (86% of the cells) or short cilia (present on 14% of the cells). Scale bar represents 5 µm. Quantification of ciliation and cilia length in MEFs: *Fop*$^{+/+}$ or *Fop*$^{gt/gt}$ MEFs were transfected with control, FOP or FOP Δ-Cter rescue plasmids (as indicated in the bottom two lanes) and starved for 24 h. Transfected cells are identified with the staining of FOP with an anti-Myc tag antibody and cilia were stained. The percentage of transfected cells with cilia was calculated from the observation of 100 to 200 cells per condition and, whenever cilia were present, we measured its length. We show the mean percentage from more than three independent experiments. Vertical bars indicate s.d. *P*-values compared with control were calculated using unpaired Student's *t*-test and indicated on the figure. **(B)** Hedgehog signaling is disrupted in *Fop* $^{gt/gt}$ MEFs. qRT-PCR data showing levels of Ptch1 and Gli1 expression in MEFs from *Fop*$^{+/+}$ or *Fop*$^{gt/gt}$ MEFs after 24 or 48 h of treatment with DMSO (ctl) +/− SAG. Average amplification and s.d. of triplicates was calculated and normalized to the house keeping gene β2-Microglobulin and statistical analysis of results was carried out using *t*-tests. **(C)** SMO can relocalize to cilia upon SHH pathway stimulation in the remaining short cilia in *Fop*$^{gt/gt}$ MEFs. MEFs from *Fop*$^{+/+}$ or *Fop*$^{gt/gt}$ were serum starved to induce ciliation and treated for 24 more h with SAG and compared to control. SMO (green) relocalization in the cilia (visualized with acetylated tubulin staining, red) was analyzed by immunofluorescence. Scale bar represents 5 µm.

GFP labeling only on a subset of satellites (Supplementary Fig. S6C). It is possible that GFP-PCM1 incorporates in all satellites but at levels below detection or, alternatively, that GFP-PCM1 incorporates in only a fraction of the satellites. We continued our study to analyze if modification of *Fop* expression would alter the organization of satellites (labeled and unlabeled). We used two siRNAs described in the literature to inhibit *Fop* expression (40). Oligo#1 reduced 91% of FOP at the centrosome in immunofluorescence (FOP was easily eradicated from satellites but its centrosome pool was more difficult to eliminate) and 100% in Western blot. Oligo#2 reduced 95% of FOP at the centrosome in immunofluorescence and 100% in Western blot (Fig. 5C, Supplementary Fig. S6D). Oligo#2 had the strongest effects. In HeLa-Kyoto cells FOP siRNA treatment induced a concentration of PCM1 satellites around the centrosome that sometimes appeared as a compact mass (Fig. 5D). This showed that FOP was also involved in the correct distribution of satellites in HeLa cells. We observed that satellites lose their gradient distribution and tended to aggregate together. The end result was different in HeLa cells (concentration around the centrosome) than in MEFs (dispersion). This could be due to the difference in cells adapting to a transient inhibition (obtained by siRNA), or to the genetic alteration of *Fop* (obtained by the gene trap). One hypothesis could be that the alteration of satellite dynamics observed in HeLa cells is an intermediate state that eventually results in what was observed in MEFs. Finally, we cannot exclude that the effects depend on the cell line used in the assay. We measured the concentration of various PCM proteins and, like in MEFs, we observed an increased amount of Pericentrin, γ-Tubulin in the PCM of FOP siRNA-treated cells (Fig. 5C). In conclusion, HeLa cells treated with FOP siRNA reproduced our main observations in MEFs and were a good model to study satellite dynamics.

We next looked at PCM1 satellite dynamics in live cells treated with control or FOP siRNA. In control cells we observed that only a small fraction of satellites moved at a given time. Satellite movements were rapid, jumpy with pauses and changes in direction (Supplementary material, Movie M1). They moved both towards and outwards from the centrosome. Two opposing activities move vesicles and cargos along MTs. Kinesins are responsible for movements from the minus- to the plus-ends of MTs (globally from the centrosome to the periphery). Their *in vitro* speed is around 0.5 µm/s (46). Cytoplasmic dyneins move cargos toward the minus-end of MTs (typically toward the cell center). Their *in vitro* speed is around 6.5 µm/s (46). Macromolecules, organelles and vesicles movements are the result of a balance between the activities of the two kinds of motors. In our recordings we could not unambiguously trace

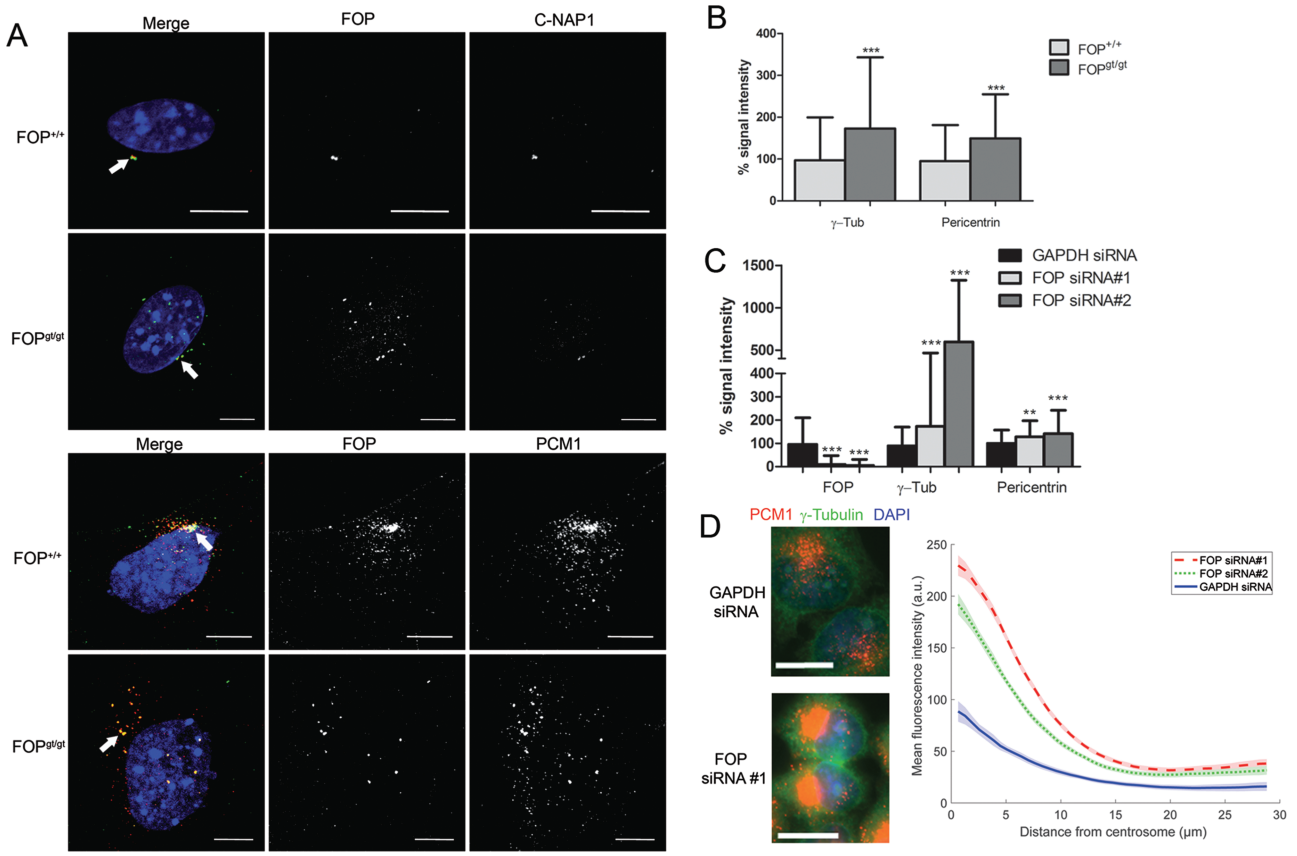

Figure 5. PCM composition and centriolar satellite defects. **(A)** Immunofluorescence of $Fop^{+/+}$, $Fop^{+/gt}$ or $Fop^{gt/gt}$ MEFs to detect FOP (wild-type and chimeric), c-Nap (as a centrosome marker) and PCM1 (as a CS marker). Centrosomes are indicated by the white arrow. Scale bar represents 10 µm. **(B)** Quantification of two PCM components in $Fop^{+/+}$ and $Fop^{gt/gt}$ MEFs. Representative result of three experiments in which the signals of γ-Tubulin and Pericentrin stainings were quantified in at least 100 cells in each condition. The histogram presents the mean total intensities relative to that in the control treated sample (mean set to 100%). Error bars show s.d. *P*-values compared with the control were calculated using unpaired Student's *t*-tests. **(C)** Quantification of FOP, γ-Tub and Pericentrin centrosomal concentration in Hela-Kyoto cells were treated with control (GAPDH), FOP siRNA#1 or FOP siRNA#2 antisense oligonucleotides. Representative result of 2 experiments in which the signals were quantified in at least 100 cells in each condition. The histogram presents the mean total intensities relative to that in the control treated sample (mean set to 100%). Error bars show s.d. *P*-values compared with the control were calculated using unpaired Student's *t*-test. **(D)** HeLa-Kyoto cells were treated with control (GAPDH) or FOP (siRNA#1) antisense oligonucleotides, fixed and stained for CS (red, PCM1), centrosomes (green, γ-Tubulin) and DNA (blue, DAPI). PMC1 gradient distribution was measured as described in the Material and Methods section. The figure shows representative pictures and graph of one of eight experiments. Scale bar represents 20 µm.

individual plus- and minus-end-directed runs. Therefore, we identified episodes of satellite motility and measured their velocities independently of their direction. Satellite speed was in average 1.66 µm/s (+/− 0.02, n = 836) with maximum peaks at 7.19 µm/s (+/− 0.12, n = 836). The velocity we observed for satellites in control cells were in line with speed measured for RAB6 secreted vesicles in cultured cells (47) or the centrosomal and CS protein AZI1/CEP131 (48).

Without MTs, in nocodazole-treated cells, the CSs were immobile, dispersed in the cells and larger (Supplementary material, Movie 2 and 49). When nocodazole was washed out, the satellites rapidly (within 2 to 10 min) became mobile and slowly regained their normal size and distribution (within 1 hour). Upon nocodazole washout and tubulin re-polymerization the satellites regained mobility independently of their size indicating that satellite aggregation in itself was not an inhibitor of the satellites mobility.

Overall, in FOP-depleted cells, we observed a reduction in both the number of satellites and their movements (number of tracks per cell) (comparison of Movie 3 (control) and Movie 4 (FOP siRNA), images from those movies are in Fig. 6A and quantification in Fig. 6B graph i). More specifically, we noticed less discrete standard-size satellites (Fig. 6Aii and B graph ii) but more 'packs'/clusters of them, in accordance with our immunofluorescence experiments. Packs of satellites were considerably bigger in FOP-depleted cells than those occasionally observed in control cells (Fig. 6B graph iii). They were much less motile than standard-size satellites (Supplementary Fig. S7 graph i) and their motions were slower (Supplementary Fig. S7 graph ii). In FOP siRNA-treated cells, the standard-size satellites were less abundant but there was no change in their ability to move in terms of movement frequency (Supplementary Fig. S7 graph iii), and no important change in speed and traveled distances compared to satellites in control cells (Supplementary Fig. S7 graph iv and v). In conclusion, the reduction of the expression of FOP induced a loss of satellite mobility and their aggregation.

Discussion

Skeletal dysplasias are a clinically and genetically heterogeneous group of bone and cartilage disorders. A total of 436

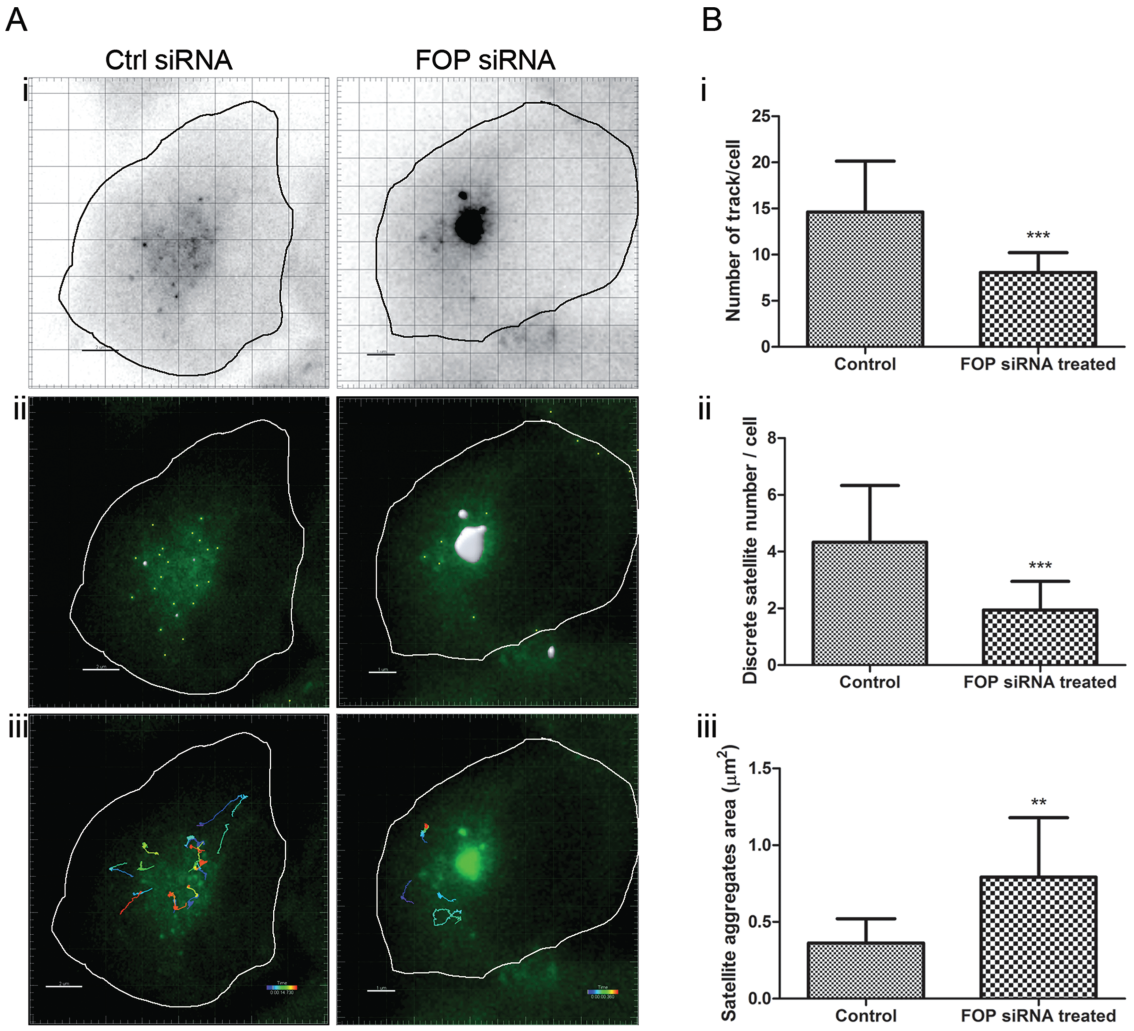

Figure 6. Centriolar satellites movements in control and FOP siRNA treated cells. **(A)** HeLa-Kyoto-GFP-PCM1 clone H4 cells treated with control (GAPDH) or FOP siRNA were filmed for 72 s. CS tracks were analyzed and we focused on CS with tracks with more than 67 spots (i.e. track that last more than 2 s) and with displacement length over 0.5 µm. For illustration we show pictures of one time frame i) before analysis, ii) highlighting satellite surfaces (yellow dots are discrete satellites and white surface are aggregates of them) and iii) showing CS tracks over the duration of the movie. The line highlights the cell border. **(B)** Quantification of CS and CS tracks characteristics. Are represented results of three independent experiments in which HeLa-Kyoto-GFP-PCM1 clone H4 cells treated with control (GAPDH) or FOP siRNA were filmed for 72 s. CS tracks were analyzed and we focused on CS with tracks with more than 67 spots (i.e. track that last more than 2 s) and with displacement length over 0.5 µm. At least 121 cells were analyzed in each condition (three independent experiments). The histogram presents the mean value per time frame, error bars show s.d. *P*-values compared with the control were calculated using unpaired Student's *t*-test. Comparison in control or FOP siRNA treated cells of i) the number of tracks per cell; ii) the number of discrete CS per cell and iii) the area of CS.

skeletal dysplasias are listed in the 2015 revised version of the nosology and classification of genetic skeletal disorders, of which nearly 20% remain genetically and molecularly uncharacterized (50). We have shown here that the mutation of the centrosomal and satellite protein FOP induces a ciliopathy in mice reminiscent of human SRPSs. SRPSs are rare bone dysplasias, lethal or not, characterized by short ribs, narrow thorax and short long bones. The other unifying feature of these syndromes is that they belong to the ciliopathy group of skeletal disorders with defects in PC formation or function (36,50). To our knowledge it is the first time that a mutant protein from the centrosome and CSs is described to produce phenotypes in mice that recapitulate a SRPS.

In humans, many of the prenatal onset skeletal dysplasias are lethal, often due to dysplasia of the thoracic cavity, which results in pulmonary hypoplasia. The mouse model we have developed reproduces this observation. The mutant mice have drastic developmental problems leading to intrauterine or perinatal death with general growth defects and, more specifically, lungs and heart hypoplasia incompatible with life. Variation in the expressivity of the phenotype is illustrated by the fact that mice die at different developmental stages and display a variable extent of the same spectrum of phenotypes. Such variability of phenotype is common in ciliopathies (51–53). Recent papers indicate that this may be due to modifier alleles that affect the degree of expression of the phenotype (54). We observed similar phenotypes in three backgrounds. This suggests a monogenic origin, and that the variation in phenotype severity may be due to differences in genomic architecture, epigenetic or other nongenetic factors in each affected individuals (55).

FOP mutations have not yet been reported in human cases of SRPS but our results in mice indicate that it should be considered

when searching for the founding genetic alteration responsible for SRPS cases. The specific mutation of *Fop* we analyzed is probably hypomorphic but already has dramatic consequences for embryonic development. It is hard to predict what would happen in a complete loss-of-function or with other types of mutations. Given the severity of the mice developmental defects it is possible that early miscarriage in humans prevents assessing FOP's role in human ciliopathies. The gene trap analyzed here reveals a rate-limiting function of FOP in certain tissues during development. Given FOP ubiquitous expression, it is possible that different mutations in this gene could lead to other forms of ciliopathies. Moreover, FOP could contribute to modify the phenotype of another ciliopathic protein mutation as it has been described for BBS mutations, which contribute to the phenotypic variation of *CEP290*-related ciliopathies (56) or for TTC21B (57).

The observed mouse developmental defects could result from centrosome- or cilia-related functions of FOP. It is established that SRPSs are ciliopathies and that the skeletal dysplasia observed in these pathologies is probably due to cilia's role in Hedgehog signal transduction (1,58–60). Previous work (41,42) and our work show that FOP is required for ciliogenesis and we show that Hedgehog signaling is impaired by *Fop* mutation, which probably explains the most apparent phenotypes observed in *Fop* mutant embryos. It is, however, possible that *Fop* mutation has other effects that do not manifest notably because of the short life span of the animals. Aside from its role in ciliogenesis, FOP also has centrosomal-related functions, e.g. it is important for cell cycle progression and MT anchoring (39,40). FOP is far from being the only protein to have both cilia-related and centrosome-related functions but joins a growing list of cilia proteins (61). Alteration of centrosome-related functions has been linked to microcephaly (32), but could contribute also to phenotypes described in ciliopathies. For example, centrosomes mature into spindle poles in mitosis and are involved in mitotic spindle organization, cell division orientation and cytokinesis. Defect in any of those functions could participate in cyst formation, developmental delay or other traits observed in ciliopathies. It is difficult to distinguish centrosome- from cilia-related functions. There is a homology in functions necessary for MT organization during ciliogenesis and during cell division, notably because they rely on shared mechanisms or constituents, such as in the case of IFT88, e.g. (62). However, the dominant phenotypes associated with defect of centrosome/cilia proteins often seem to be linked to their role in cilia function [ex IFT88 (63), OFIP (30)].

Fop is ubiquitously expressed in the embryo but the ciliogenesis defect is not uniform and in every tissue. This variation in the penetrance of the phenotype commonly seen for 'core' centrosomal genes could have various explanations. There could be redundant mechanism(s) that compensate for its mutation in certain tissues. In constitutive mutant animal models, compensation mechanisms are more likely to be implemented than in experiments in which the deficiency is only transient (e.g. with acute knockdown by RNA interference). This has been clearly shown for the centrosomal and CS protein AZI1/CEP131 (48). AZI1 is essential for PC formation in various *in vitro* settings (25,48,64) but *Azi1*-null mice or MEFs derived from it do not display anomaly of cilia formation. The only phenotype of those mutant mice is male infertility, due to impaired formation of the modified cilia of the sperm flagella (48). In our model it is possible that compensation mechanisms exist to counterbalance *Fop* mutation, but only in certain cells. It is also possible that the gene trap corresponds to a hypomorphic mutation and the specific defects we observed highlight sensitivity of some tissues to a rate limiting function of FOP during development, especially for SHH signaling in certain tissues. Another aspect to take into account is that even if the building of cilia is coined under the collective term of ciliogenesis, some mechanisms must be specific to certain tissues. How the core ciliary assembly program is modified and elaborated on to account for these cell-specific variations is not well understood, and the machinery necessary for the formation of different kinds of cilia may vary. For example, one of the functions of the BBSome is to promote cilia membrane biogenesis through the small GTPase RAB8. However, in the absence of one of its component, BBS7, Polycystin-1 and -2 are correctly addressed in kidney cells when Dopamine D1 receptor abnormally accumulates in the ciliary membrane in the brain (56). Different types of ciliogenesis may be required to create different cilia and FOP may be specifically required for the formation of some but not all cilia.

The phenotype of heterozygous $Fop^{+/gt}$ mice is somewhat surprising. Contrary to homozygous embryos, heterozygous $Fop^{+/gt}$ mice do not present skeletal defects but obesity. Among ciliopathies this phenotype is a characteristic of BBS, and to a lower extent Joubert Syndrome, but not SRPS (65). However, the link between ciliary dysfunction and metabolic deregulation leading to obesity is well established but complex (66,67). $Fop^{+/gt}$ mice may present cilia dysfunction in the adult, which is known to cause obesity, even in nonhomozygous situations (67–71). Of note, one of the other common symptoms of cilia dysfunction in postnatal life is kidney disease, which we never observed in $Fop^{+/gt}$ mice. Recent studies show how proteins localized to the cilia of neurons in the hypothalamus control food intake in mice. Notably, mice heterozygous null for ADCY3, a neuronal primary cilium adenylyl cyclase possibly involved in the leptin-melanocortin pathway, have increased susceptibility to obesity (67,70,71). It is possible that reduced localization of ADCY3 at PC contributes to obesity in $Fop^{+/gt}$ mice. Interestingly, as an alternative, but not exclusive possibility, alteration of CSs in hypothalamic neurons due to heterozygous FOP mutation may deregulate autophagy, which is known to control food intake (66,72).

To assess FOP function in ciliogenesis we looked at its role as part of a complex with CAP350 and EB1 (40). Centrosomal/basal body localization of EB1 is important for ciliogenesis (73,74) and, in a work looking at MT anchoring at the centrosome, it was shown to be dependent on a complex of EB1 with CAP350 and FOP. Yet, the mutant form of FOP expressed in the FOP gene trap mice lacks the interaction domain with EB1 [(40) and our own immunoprecipitation and immunofluorescence data]. EB1 recruitment to the centrosome/basal body may be affected by FOP mutation, which may explain the defect in ciliogenesis. If MT anchoring was lost at the centrosome because of EB1 absence, MT disorganization could also perturb the traffic of satellites. We analyzed this hypothesis in MEFs derived from gene-trapped mice and did not observe any MT disorganization and no anchoring problems (data not shown). EB1 localization at the centrosome was, however, difficult to observe, even in wild-type cells. It thus appears that in primary mouse fibroblasts CAP350-EB1-FOP does not have the same functions in MT anchoring as described in another context, and that a perturbation of this complex cannot account for the ciliogenesis defect, at least in MEFs.

FOP also localizes at CSs and perturbs their distribution, thus we wanted to know if this could explain how ciliogenesis is perturbed. The mechanisms connecting CSs to cilia formation remain to be completely elucidated, but multiple satellite proteins are essential contributors to ciliopathies and CSs are suggested assembly points for cilia proteins (21,27,75). For

example, BBS4 on CSs regulates the recruitment of the BBSome into the cilia, which in turn regulates IFT, a central actor in cilia building and function (14). CS proteins like CEP72 and CEP290 also control the accumulation of RAB8, another important player in cilia formation (19,76). In most cases the depletion or mutation of one of the satellite proteins affects the presence of other proteins at CSs (20,21,30,49,77). This is often associated with the loss of CS integrity and is accounted responsible for faulty ciliogenesis. In our case, however, FOP mutation or depletion did not inhibit the recruitment of proteins to the CSs (PCM1, OFD1, CEP290 and FOR20 were tested) but affected the intrinsic property of satellites to move along MTs, and we have shown that altering this function leads to a perturbed balance of PCM composition and can lead to ciliopathic defects. Other satellite proteins having a conserved N-terminal part similar to FOP (OFD1, FOR20) were proposed to be involved in satellite dynamics control and ciliogenesis (49,72,78–80). Our results show that the N-terminal part of FOP containing the LisH homodimerization domain (conserved in the gene trap) is sufficient to restore ciliogenesis to control levels in $Fop^{gt/gt}$ MEFs. In the case of the *Fop* gene trap mutant, the addition of the large β-gal entity to the protein probably impairs the functionality of the N-terminal domain by altering its interaction with other proteins. Defining precisely the functional and structural role of this conserved region is of great interest and will require further study.

Materials and Methods

Mouse colony care, $Fop^{+/gt}$ generation, genotyping and breeding

All mice were housed and maintained in a specific pathogen-free environment. Breeding, monitoring and experimental procedures were performed in accordance with the French Guidelines for Animal Handling.

129/Ola ES cells carrying a gene-trap vector pGT0lxr in intron 4 of *Fop* were obtained from the Wellcome Trust Sanger Institute (Cambridge, UK). Mutant mice were produced using standard procedures after microinjection of the mutated stem cells in C57BL/6 blastocysts.

Genotyping primers were as follows:

1-FOP1 S	5′-CAAGGTCTTGAAGGTCGAGAGAAC-3′
2-FOP5 AS	5′-TCCATCAGTGACGCTCTCTATGC-3′
3-betaGEO AS	5′-ATTCAGGCTGCGCAACTGTTGGG-3′
4-EN2Int1 S	5′- GGTTTAGCTACATCTGCCAATCCA-3′

PCR primers 1 (FOP1 S) and 2 (FOP5 AS) are used to generate a 713 bp product from the wild-type allele and primers 3 (betaGEO AS) and 4 (EN2Int1 S) produce a 503 bp product from the gene-trapped allele.

Thermal cycler PCR conditions were 98°C for 3 min followed by 35 cycles of 98°C for 10 s, 60°C for 10 s and 72°C for 15 s and performed using the Phire II DNA Polymerase (Thermo Fisher Scientific).

MEFs preparation

MEFs were established from $Fop^{gt/gt}$, $Fop^{+/gt}$ and $Fop^{+/+}$ E14.5 embryos using the following procedure. Briefly, embryos were dissected and heads and visceral organs were removed and kept for genotyping. The remaining tissue was placed in a tissue culture dish containing Dulbecco's modified Eagle's medium supplemented with 10% fetal bovine serum (FBS) (Gibco) and 1% penicilin/streptomycin (Gibco), 1% β-mercaptoethanol (Sigma), 1% sodium pyruvate (Gibco) and 1% nonessential amino acids (Gibco). Tissue was dissociated by scraping tissue through nylon membrane using a round bottom forceps. The resulting cell suspension was transferred in a 15 ml tube and complete to 10 ml with medium. Further homogenization was obtained by pipetting up and down 10 times the suspension. The largest remaining aggregates were eliminated by decantation. The solution was then filtered on 70 µM membrane, centrifuged and placed in fresh medium. Consecutively, cells were plated on 10 cm dishes.

Reverse transcription and RT-PCR

RNAs were extracted with Trizol (Thermo Fisher Scientific) from MEFs following the supplier protocol. 2 µg of RNA was used for reverse transcription. Random primer reverse transcription was done with Superscript II reverse transcriptase (Thermo Fisher Scientific). PCR assays to detect wild-type (Fop^{+}) and fused FOP-β-Geo (Fop^{gt}) allele were done on cDNA using the following primers: FOP1 S, FOP5 AS and betaGEO AS. β-actin was used as a control of the cDNA amount for each sample. The corresponding primers are described below. The resulting PCR product is a 646 bp fragment.

Murine betaActinS 5′- CCTAAGGCCAACCGTGAAAAG - 3′
Murine betaActinAS 5′- TGGCTCCTAGCACCATGAAGA - 3′

Skeletal preparation and staining

Alcian blue and alizarin red staining was done using standard protocols. Briefly mice were eviscerated, fixed in 95% ethanol for 2 days, kept in acetone for 2 days and rinsed with water. Staining cocktail (1 volume 0.3% alcian blue in 70% EtOH, 1 volume 0.1% alizarin red in 95% EtOH and 1 volume 100% acetic acid in 17 volume 100% EtOH) was added and incubated at 37°C for 5–10 days until bones became visible through surrounding tissue and fully stained. Surrounding tissue was cleared by immersion in 1% KOH for 24 h followed by graded 1% KOH/glycerol series. Stained skeletal preparations were stored and photographed in 100% glycerol.

X-gal staining

Embryos were fixed on ice in a fixative solution containing 2% formaldehyde, 0.2% glutaraldehyde in phosphate buffered saline (PBS). Consecutively, samples were washed three times with 100 mM sodium phosphate buffer (pH 7.3), 2 mM magnesium chloride, 0.02% Nonidet P-40 and 0.01% sodium deoxycholate. Embryos were stained for lacZ activity with a reaction buffer containing 1 mg/ml X-gal, 5 mM potassium ferricyanide, 5 mM potassium ferrocyanide, 100 mM sodium phosphate buffer (pH 7.3), 2 mM magnesium chloride, 0.02% Nonidet P-40 and 0.01% sodium deoxycholate. After staining, embryos were washed again three times then post fixed with 3.7% formaldehyde in PBS.

For cryostat sectioning, embryos were washed in PBS, incubate overnight in 25% sucrose solution and then immersed in optimal cutting temperature (OCT) embedding matrix (CellPath) and frozen on dry ice. Cryosections (12 µm) were stained for lacZ activity according to the previous indications and counterstained with nuclear fast red (Sigma-Aldrich). Consecutively, sections were dehydrated, immersed in Histolemon (ErbaRS) and mounted in Pertex Mounting Medium (Histolab).

Northern blot analysis

Twenty micrograms of total RNA from MEFs were separated on a 1.5% agarose gel, blotted on Hybond-N (Amersham GE Healthcare) and hybridized according to Church and Gilbert (81). The probe corresponds to nucleotides 383–596 of mouse *Fgfr1op* cDNA (NCBI Reference Sequence: NM_001197046.1).

SHH signaling induction, Q-RT-PCR

MEF established from $Fop^{+/+}$ or $Fop^{gt/gt}$ E14.5 embryos were starved O/N in 0.3% FBS, then treated 24 or 48 h with 100 nM of Smoothened Agonist (SAG, Calbiochem) or dimethylsulfoxyde (DMSO) alone. Cells were fixed for immunofluorescence and RNAs were extracted with RNeasy Plus Mini Kit (Qiagen), reverse transcribed using Transcriptor High Fidelity cDNA Synthesis Kit (Roche). Quantitative real-time PCR was carried out using Sybr Green (Life Technologies) and run on 7500 Real-Time PCR System (Applied Biosystem). Primer sets used were as follows:

β2-Microglobulin	5′- CCGTTCTTCAGCATTTGGAT-3′
β2-Microglobulin	5′- CTGACCGGCCTGTATGCTAT-3′
ptch1-rt-f	5′- CTGGCAGCCGAGACAAGCCC-3′
ptch1-rt-r	5′- TGGCCTGGGAGGCAGCGTAA-3′
gli1-rt-f	5′- GCCAGCTGGAGGTCTGCGTG-3′
gli1-rt-r	5′- TGGCTGTGGAGGGGTCGGAG-3′

Data were normalized to the house-keeping gene β2-Microglobulin. ΔCT was calculated for each sample as ΔCT = CT(sample)-Average CT(house keeping gene); amplification = 2^-ΔCT for each sample; average amplification and standard deviation (s.d.) of triplicates was calculated and statistical analysis of results was carried out using *t*-tests.

Cells, antibodies and reagents

Cells were cultured at 37°C and 5% CO2. Hela-Kyoto mPCM1-GFP were obtained from the Max Planck Institute of Molecular Cell Biology and Genetics (Dresden, Germany). They were grown in DMEM high glucose (Life Technologies) supplemented with penicillin–streptomycin, 10% FBS and 400 ug/ml G418. MEFs were grown in DMEM high glucose supplemented with penicillin–streptomycin, 10% FCS, 1% sodium pyruvate, 1% nonessential amino acids and 0.125 mM β-Mercaptoethanol. For induction of cilia formation MEF were serum starved for 24 h.

The following antibodies used in this study were from Sigma-Aldrich: anti-γ-Tub antibodies [mouse monoclonal GTU-88 (T6557) and rabbit polyclonal T3559 (T3559)] and anti-acetylated tubulin mouse monoclonal (IgG_{2b})(6-11B-1)(T7451); from Proteintech: anti-FOP antibodies rabbit polyclonal (11343–1-AP) and anti-ARL13 rabbit polyclonal (17711–1-AP); from Abcam: anti-glyceraldehyde 3-phosphate dehydrogenase (GAPDH) mouse monoclonal 6C5 (ab8245), anti-Pericentrin rabbit polyclonal, anti-GFP antibodies rabbit polyclonal (ab290) and mouse monoclonal 9F9 (ab1218); from Millipore: anti-detyrosinated tubulin (Glu-Tub) rabbit polyclonal (AB3201) and anti-Centrin mouse monoclonal 20H5 (04–1624); from Santa Cruz Biotechnology: mouse anti-c-Myc (9E10)(SC-40), mouse anti-Smo (IgG_{2a})(E-5)(SC-166685); from Promega: anti-β-Gal mouse monoclonal (Z3783); from Abnova: anti-FOP antibodies used were a mouse monoclonal 2B1 (157H00011116-M01); from BD Transduction Laboratories: anti-c-Nap1 mouse monoclonal (611374) and from Bethyl Laboratories: rabbit polyclonal anti-PCM1 (A301-150A).

Statistical data analysis

Statistical data analysis was done with the GraphPad Prism software. All data are presented as mean of multiple experiments +/− s.d. Experiment sample numbers and the number of replicates used for statistical testing has been reported in the corresponding figure legends. All *P*-values are from two-tailed unpaired student's *t*-tests. Unless otherwise stated we followed this key for asterisk placeholders for *P*-values in the figures; $^{***}P < 0.001$, $^{**}P < 0.01$, $^{*}P < 0.05$ and ns = non-significant.

PCM1 gradient measurement

For each siRNA condition, 8 RGB-images were acquired (Zeiss Apotome microscope) at a magnification of 40x (Plan-Neofluar 40x/1.30 Oil Objective), corresponding to a pixel size of 0.16 µm. Centrosomes were manually localized and their position was saved as a white dot on a supplementary layer of the image. The gradient of PCM1 distribution around centrosomes was computed as follows: for each image, the mean fluorescence intensity was computed over pixels localized at equidistance from the centrosomes, with a distance gradually increasing, starting from 0 to 30 µm (20 µm corresponding to the average cell size). Gradients of fluorescence distribution are displayed as mean and s.d.

Videomicroscopy and CS track analysis

The day before filming HeLa-Kyoto-mPCM1-GFP cells treated with control or FOP siRNA were seeded on glass bottom plates (Cellview, Greiner). Before filming cells were transferred in DMEMgfp (Evrogen) + 10 mM Hepes in a large CO2- and thermo-controlled chamber on an Axio Observer Z1 microscope (Zeiss). Cells were illuminated with a 491 nm Roper Scientific Ilas2 laser and wide field images were acquired every 30 ms for 72 s with a 63/1.46 alpha plan Apochromat objective with EM-CCD Evolve 512 Camera (photometrics). Acquisitions were driven by Metamorph 7.8 Software (Molecular Device). Analysis was done with Imaris (Bitplane AG) Software. CSs were identified by the 'spots' and 'surface' functions. To avoid measuring unspecific background signals, we concentrated on spots that could be detected for more than 2 s. To discriminate 'discrete' and 'aggregates' we used the diameter of the sphere (cut of under 0.1 µm for 'discrete' and 0.6 µm for 'aggregates') and an arbitrary cutoff of the 'quality' (the intensity of a Gaussian-filtered channel from above minus the intensity of the original channel Gaussian filtered by 8/9 of spot radius). To analyze CS dynamics we used the 'track spot' function with the autoregressive motion algorithm, a maximum gap size of 4, maximum distance 0.4 µm. We focused on track that lasted more than 2 s (tracks of more than 67 time points). To remove background movements we considered tracks with displacement length over 0.5 µm.

Plasmid construction and cell transfections

For plasmids, MEFs were electroporated with Nucleofector technology (Lonza) according to the supplier's protocol.

The sequence coding for the full-length and truncated (FOP Δ-Cter) proteins were amplified by PCR using Platinum HiFi polymerase (Invitrogen) and Gateway-compatible primers and transferred into pDONR/ZEO using Gateway technology-mediated recombination. The sequences were subsequently transferred by recombination into modified Gateway-compatible pRK5/Myc.

siRNA oligonucleotides were transfected with RNAiMax reagent (Thermo Fisher) according to the manufacturer's protocol. The sequences are the following: FOP siRNA #1 (5′-UUGACAGCGCCUGAUCACUUUU -3′), FOP siRNA #2 (5′-UAAAUUCUCUCGACCUUCGAGUU -3′). siRNAs, including control GAPDH, were purchased from Dhamacon as ON-TARGETplus siRNAs.

Immunofluorescence and fluorescence quantification

Cells were grown on coverslips, fixed in cold methanol for 5 min at −20°C and rinsed in PBS. After blocking in PBS-3% bovine serum albumin (BSA) 15 min cells were incubated 1 h with appropriate mixture of primary antibodies. After washing in PBS they were incubated 1 h with the adequate secondary antibodies conjugated to Cy2, Cy3, Cy5 (Jackson Laboratories). DNA was stained with 250 ng/ml DAPI. After washing, cells were mounted in Prolong Gold Antifade reagent (Life Technologies). Slides were examined on an LSM-510 Carl Zeiss confocal microscope with an x63 NA1.4 Plan Apochromat. Z-series optical sections were obtained at 0.2 µm steps and then projected with LSM software (Zeiss) as maximum projections. Images were processed using Photoshop 8.0.1. For quantification of fluorescence signals, images were acquired on an Apotome microscope (Zeiss) and image quantification was done with ImageJ Software. Each centrosome was marked by a circle region of interest (ROI), signal was identified by thresholding with identical limits in all conditions and fluorescence measured within the threshold in the ROI. Background fluorescence was measured in close proximity. Fluorescence at the centrosome of protein x = integrated density of protein x– (mean background*measured area) = measured area *(mean value protein x – mean value background).

Immunofluorescence on tissue sections

Tissues were fixed in 4% paraformaldehyde overnight at 4°C, rinsed in PBS, incubated in 30% sucrose overnight at 4°C, included and frozen in OCT embedding matrix (Cellpath). Cryosections (12 µm) were obtained on a Leica CM30505S cryotome and processed for immunohistochemistry. Slides were rehydrated in PBS, permeabilized for 10 minutes in PBS/0.2% Triton X-100, saturated for 30 minutes in PBS-3% BSA. Slides were incubated in the same buffer with appropriate mixture of primary antibody overnight at RT, rinsed in PBS, incubated 2 hours with Cy-coupled secondary antibodies (Jackson Laboratories) and 250 ng/ml DAPI. Slides were rinsed in PBS and mounted in Prolong Gold Antifade mounting medium (Life Technologies) before observation on a LSM-510 Carl Zeiss confocal microscope with a 63 NA1.4 Plan Apochromatic objective and driven by Zen 2009 software. Images were processed using Photoshop 8.0.1.

Cell extracts and Western blot analysis

Cells were harvested and washed in PBS, lysed in RIPA buffer (50 mM Tris–HCl pH 8, 150 mM NaCl, 0.1% SDS, 1% NP40, 0.5% sodium deoxycholate) and a complete ethylene diamine tetraacetic acid (EDTA)-free protease inhibitor cocktail (Roche Applied Science) for 30 min on ice. Clear lysate were obtained after 10 min centrifugation at 4°C and 13 000 rpm and protein concentration was measured by Bradford protein assay (Biorad). 50 µg of cell extracts were run in polyacrylamide gels and transferred on to Hybond^{TM}-C membrane (GE Healthcare Life Science) followed by detection with antibodies.

Supplementary Material

Supplementary Material is available at *HMG* online.

Acknowledgements

This work was supported by Institut National de la Santé et de la Recherche Médicale (INSERM) and Institut Paoli-Calmettes. We are grateful to Dr Valérie Cormier Daire for a stimulating discussion. We thank Ina Poser and Anthony Hyman (Max Planck Institute of Molecular Cell Biology and Genetics, Dresden, Germany) for the TransgeneOmics cell line and BAC construct. We are grateful to Daniel Isnardon for assistance with the use of the Misc. Imaging facility and we are grateful for the technical support of the animal facility especially Sylvie Marchetto and Jean-Christophe Orsoni.

Conflict of Interest statement. None declared.

References

1. Wong, S.Y. and Reiter, J.F. (2008) The primary cilium at the crossroads of mammalian hedgehog signaling. *Curr. Top. Dev. Biol.*, **85**, 225–260.
2. Gerdes, J.M. and Katsanis, N. (2008) Ciliary function and Wnt signal modulation. *Curr. Top. Dev. Biol.*, **85**, 175–195.
3. Singla, V. and Reiter, J.F. (2006) The primary cilium as the cell's antenna: signaling at a sensory organelle. *Science*, **313**, 629–633.
4. Nigg, E.A. and Stearns, T. (2011) The centrosome cycle: centriole biogenesis, duplication and inherent asymmetries. *Nat. Cell Biol.*, **13**, 1154–1160.
5. Ishikawa, H. and Marshall, W.F. (2011) Ciliogenesis: building the cell's antenna. *Nat. Rev. Mol. Cell. Biol.*, **12**, 222–234.
6. Al Jord, A., Lemaitre, A.I., Delgehyr, N., Faucourt, M., Spassky, N. and Meunier, A. (2014) Centriole amplification by mother and daughter centrioles differs in multiciliated cells. *Nature*, **516**, 104–107.
7. Wang, W., Wu, T. and Kirschner, M.W. (2014) The master cell cycle regulator APC-Cdc20 regulates ciliary length and disassembly of the primary cilium. *Elife*, **3**, e03083.
8. Parker, J.D., Hilton, L.K., Diener, D.R., Rasi, M.Q., Mahjoub, M.R., Rosenbaum, J.L. and Quarmby, L.M. (2010) Centrioles are freed from cilia by severing prior to mitosis. *Cytoskeleton (Hoboken)*, **67**, 425–430.
9. Paridaen, J.T., Wilsch-Brauninger, M. and Huttner, W.B. (2013) Asymmetric inheritance of centrosome-associated primary cilium membrane directs ciliogenesis after cell division. *Cell*, **155**, 333–344.
10. Sanchez, I. and Dynlacht, B.D. (2016) Cilium assembly and disassembly. *Nat. Cell Biol.*, **18**, 711–717.
11. Lechtreck, K.F. (2015) IFT-Cargo Interactions and Protein Transport in Cilia. *Trends Biochem. Sci.*, **40**, 765–778.
12. Pedersen, L.B. and Rosenbaum, J.L. (2008) Intraflagellar transport (IFT) role in ciliary assembly, resorption and signalling. *Curr. Top. Dev. Biol.*, **85**, 23–61.
13. Garcia-Gonzalo, F.R. and Reiter, J.F. (2017) Open sesame: how transition fibers and the transition zone control ciliary composition. *Cold Spring Harb. Perspect. Biol.*, **9**, 10.1101/cshperspect.a028134.
14. Wei, Q., Zhang, Y., Li, Y., Zhang, Q., Ling, K. and Hu, J. (2012) The BBSome controls IFT assembly and turnaround in cilia. *Nat. Cell Biol.*, **14**, 950–957.

15. Pedersen, L.B. and Christensen, S.T. (2012) Regulating intraflagellar transport. *Nat. Cell Biol.*, **14**, 904–906.
16. Jin, H., White, S.R., Shida, T., Schulz, S., Aguiar, M., Gygi, S.P., Bazan, J.F. and Nachury, M.V. (2010) The conserved Bardet–Biedl syndrome proteins assemble a coat that traffics membrane proteins to cilia. *Cell*, **141**, 1208–1219.
17. Nachury, M.V., Loktev, A.V., Zhang, Q., Westlake, C.J., Peranen, J., Merdes, A., Slusarski, D.C., Scheller, R.H., Bazan, J.F., Sheffield, V.C. *et al.* (2007) A core complex of BBS proteins cooperates with the GTPase Rab8 to promote ciliary membrane biogenesis. *Cell*, **129**, 1201–1213.
18. Barenz, F., Mayilo, D. and Gruss, O.J. (2011) Centriolar satellites: busy orbits around the centrosome. *Eur. J. Cell Biol.*, **90**, 983–989.
19. Stowe, T.R., Wilkinson, C.J., Iqbal, A. and Stearns, T. (2012) The centriolar satellite proteins Cep72 and Cep290 interact and are required for recruitment of BBS proteins to the cilium. *Mol. Biol. Cell*, **23**, 3322–3335.
20. Wang, L., Lee, K., Malonis, R., Sanchez, I. and Dynlacht, B.D. (2016) Tethering of an E3 ligase by PCM1 regulates the abundance of centrosomal KIAA0586/Talpid3 and promotes ciliogenesis. *Elife*, **5**, 10.7554/eLife.12950.
21. Lopes, C.A., Prosser, S.L., Romio, L., Hirst, R.A., O'Callaghan, C., Woolf, A.S. and Fry, A.M. (2011) Centriolar satellites are assembly points for proteins implicated in human ciliopathies, including oral-facial-digital syndrome 1. *J. Cell Sci.*, **124**, 600–612.
22. Kodani, A., Yu, T.W., Johnson, J.R., Jayaraman, D., Johnson, T.L., Al-Gazali, L., Sztriha, L., Partlow, J.N., Kim, H., Krup, A.L. *et al.* (2015) Centriolar satellites assemble centrosomal microcephaly proteins to recruit CDK2 and promote centriole duplication. *Elife*, **4**, 10.7554/eLife.07519.
23. Firat-Karalar, E.N., Rauniyar, N., Yates, J.R. 3rd, and Stearns, T. (2014) Proximity interactions among centrosome components identify regulators of centriole duplication. *Curr. Biol.*, **24**, 664–670.
24. Balczon, R., Bao, L. and Zimmer, W.E. (1994) PCM-1, A 228-kD centrosome autoantigen with a distinct cell cycle distribution. *J. Cell Biol.*, **124**, 783–793.
25. Staples, C.J., Myers, K.N., Beveridge, R.D., Patil, A.A., Howard, A.E., Barone, G., Lee, A.J., Swanton, C., Howell, M., Maslen, S. *et al.* (2014) Ccdc13 is a novel human centriolar satellite protein required for ciliogenesis and genome stability. *J. Cell Sci.*, **127**, 2910–2919.
26. Villumsen, B.H., Danielsen, J.R., Povlsen, L., Sylvestersen, K.B., Merdes, A., Beli, P., Yang, Y.G., Choudhary, C., Nielsen, M.L., Mailand, N. *et al.* (2013) A new cellular stress response that triggers centriolar satellite reorganization and ciliogenesis. *EMBO J.*, **32**, 3029–3040.
27. Tollenaere, M.A., Mailand, N. and Bekker-Jensen, S. (2015) Centriolar satellites: key mediators of centrosome functions. *Cell. Mol. Life Sci.*, **72**, 11–23.
28. Gupta, G.D., Coyaud, E., Goncalves, J., Mojarad, B.A., Liu, Y., Wu, Q., Gheiratmand, L., Comartin, D., Tkach, J.M., Cheung, S.W. *et al.* (2015) A dynamic protein interaction landscape of the human centrosome-cilium interface. *Cell*, **163**, 1484–1499.
29. Klinger, M., Wang, W., Kuhns, S., Barenz, F., Drager-Meurer, S., Pereira, G. and Gruss, O.J. (2013) The novel centriolar satellite protein SSX2IP targets Cep290 to the ciliary transition zone. *Mol. Biol. Cell.*, **4**, 495–507.
30. Chevrier, V., Bruel, A.L., Van Dam, T.J., Franco, B., Lo Scalzo, M., Lembo, F., Audebert, S., Baudelet, E., Isnardon, D., Bole, A. *et al.* (2016) OFIP/KIAA0753 forms a complex with OFD1 and FOR20 at pericentriolar satellites and centrosomes and is mutated in one individual with oral-facial-digital syndrome. *Hum. Mol. Genet.*, **25**, 497–513.
31. Badano, J.L., Mitsuma, N., Beales, P.L. and Katsanis, N. (2006) The ciliopathies: an emerging class of human genetic disorders. *Annu. Rev. Genomics Hum. Genet.*, **7**, 125–148.
32. Chavali, P.L., Putz, M. and Gergely, F. (2014) Small organelle, big responsibility: the role of centrosomes in development and disease. *Philos. Trans. R. Soc. Lond. B. Biol. Sci.*, **369**.
33. Goetz, S.C. and Anderson, K.V. (2010) The primary cilium: a signalling centre during vertebrate development. *Nat. Rev. Genet.*, **11**, 331–344.
34. Bettencourt-Dias, M., Hildebrandt, F., Pellman, D., Woods, G. and Godinho, S.A. (2011) Centrosomes and cilia in human disease. *Trends Genet.*, **27**, 307–315.
35. Sharma, N., Berbari, N.F. and Yoder, B.K. (2008) Ciliary dysfunction in developmental abnormalities and diseases. *Curr. Top. Dev. Biol.*, **85**, 371–427.
36. Huber, C. and Cormier-Daire, V. (2012) Ciliary disorder of the skeleton. *Am. J. Med. Genet. C. Semin. Med. Genet.*, **160C**, 165–174.
37. Popovici, C., Zhang, B., Gregoire, M.J., Jonveaux, P., Lafage-Pochitaloff, M., Birnbaum, D. and Pebusque, M.J. (1999) The t(6;8)(q27;p11) translocation in a stem cell myeloproliferative disorder fuses a novel gene, FOP, to fibroblast growth factor receptor 1. *Blood*, **93**, 1381–1389.
38. Delaval, B., Letard, S., Lelievre, H., Chevrier, V., Daviet, L., Dubreuil, P. and Birnbaum, D. (2005) Oncogenic tyrosine kinase of malignant hemopathy targets the centrosome. *Cancer Res.*, **65**, 7231–7240.
39. Acquaviva, C., Chevrier, V., Chauvin, J.P., Fournier, G., Birnbaum, D. and Rosnet, O. (2009) The centrosomal FOP protein is required for cell cycle progression and survival. *Cell Cycle*, **8**, 1217–1227.
40. Yan, X., Habedanck, R. and Nigg, E.A. (2006) A complex of two centrosomal proteins, CAP350 and FOP, cooperates with EB1 in microtubule anchoring. *Mol. Biol. Cell*, **17**, 634–644.
41. Lee, J.Y. and Stearns, T. (2013) FOP is a centriolar satellite protein involved in ciliogenesis. *PLoS One*, **8**, e58589.
42. Mojarad, B.A., Gupta, G.D., Hasegan, M., Goudiam, O., Basto, R., Gingras, A.C. and Pelletier, L. (2017) CEP19 cooperates with FOP and CEP350 to drive early steps in the ciliogenesis programme. *Open Biol.*, **7**, 10.1098/rsob.170114.
43. Huangfu, D., Liu, A., Rakeman, A.S., Murcia, N.S., Niswander, L. and Anderson, K.V. (2003) Hedgehog signalling in the mouse requires intraflagellar transport proteins. *Nature*, **426**, 83–87.
44. Zhang, Q., Murcia, N.S., Chittenden, L.R., Richards, W.G., Michaud, E.J., Woychik, R.P. and Yoder, B.K. (2003) Loss of the Tg737 protein results in skeletal patterning defects. *Dev. Dyn.*, **227**, 78–90.
45. Poser, I., Sarov, M., Hutchins, J.R., Heriche, J.K., Toyoda, Y., Pozniakovsky, A., Weigl, D., Nitzsche, A., Hegemann, B., Bird, A.W. *et al.* (2008) BAC TransgeneOmics: a high-throughput method for exploration of protein function in mammals. *Nat. Methods*, **5**, 409–415.
46. Vale, R.D., Malik, F. and Brown, D. (1992) Directional instability of microtubule transport in the presence of kinesin and dynein, two opposite polarity motor proteins. *J. Cell Biol.*, **119**, 1589–1596.
47. Schlager, M.A., Serra-Marques, A., Grigoriev, I., Gumy, L.F., Esteves da Silva, M., Wulf, P.S., Akhmanova, A. and Hoogenraad, C.C. (2014) Bicaudal d family adaptor proteins

control the velocity of Dynein-based movements. *Cell Rep.*, **8**, 1248–1256.
48. Hall, E.A., Keighren, M., Ford, M.J., Davey, T., Jarman, A.P., Smith, L.B., Jackson, I.J. and Mill, P. (2013) Acute versus chronic loss of mammalian Azi1/Cep131 results in distinct ciliary phenotypes. *PLoS Genet.*, **9**, e1003928.
49. Sedjai, F., Acquaviva, C., Chevrier, V., Chauvin, J.P., Coppin, E., Aouane, A., Coulier, F., Tolun, A., Pierres, M., Birnbaum, D. *et al.* (2010) Control of ciliogenesis by FOR20, a novel centrosome and pericentriolar satellite protein. *J. Cell Sci.*, **123**, 2391–2401.
50. Bonafe, L., Cormier-Daire, V., Hall, C., Lachman, R., Mortier, G., Mundlos, S., Nishimura, G., Sangiorgi, L., Savarirayan, R., Sillence, D. *et al.* (2015) Nosology and classification of genetic skeletal disorders: 2015 revision. *Am. J. Med. Genet. A.*, **167A**, 2869–2892.
51. Alby, C., Piquand, K., Huber, C., Megarbane, A., Ichkou, A., Legendre, M., Pelluard, F., Encha-Ravazi, F., Abi-Tayeh, G., Bessieres, B. *et al.* (2015) Mutations in KIAA0586 cause lethal ciliopathies ranging from a hydrolethalus phenotype to short-rib polydactyly syndrome. *Am. J. Hum. Genet.*, **97**, 311–318.
52. Shaheen, R., Shamseldin, H.E., Loucks, C.M., Seidahmed, M.Z., Ansari, S., Ibrahim Khalil, M., Al-Yacoub, N., Davis, E.E., Mola, N.A., Szymanska, K. *et al.* (2014) Mutations in CSPP1, encoding a core centrosomal protein, cause a range of ciliopathy phenotypes in humans. *Am. J. Hum. Genet.*, **94**, 73–79.
53. Tuz, K., Bachmann-Gagescu, R., O'Day, D.R., Hua, K., Isabella, C.R., Phelps, I.G., Stolarski, A.E., O'Roak, B.J., Dempsey, J.C., Lourenco, C. *et al.* (2014) Mutations in CSPP1 cause primary cilia abnormalities and Joubert syndrome with or without Jeune asphyxiating thoracic dystrophy. *Am. J. Hum. Genet.*, **94**, 62–72.
54. Zhang, Y., Seo, S., Bhattarai, S., Bugge, K., Searby, C.C., Zhang, Q., Drack, A.V., Stone, E.M. and Sheffield, V.C. (2014) BBS mutations modify phenotypic expression of CEP290-related ciliopathies. *Hum. Mol. Genet.*, **23**, 40–51.
55. McInerney-Leo, A.M., Schmidts, M., Cortes, C.R., Leo, P.J., Gener, B., Courtney, A.D., Gardiner, B., Harris, J.A., Lu, Y., Marshall, M. *et al.* (2013) Short-rib polydactyly and Jeune syndromes are caused by mutations in WDR60. *Am. J. Hum. Genet.*, **93**, 515–523.
56. Zhang, Q., Nishimura, D., Vogel, T., Shao, J., Swiderski, R., Yin, T., Searby, C., Carter, C.S., Kim, G., Bugge, K. *et al.* (2013) BBS7 is required for BBSome formation and its absence in mice results in Bardet–Biedl syndrome phenotypes and selective abnormalities in membrane protein trafficking. *J. Cell Sci.*, **126**, 2372–2380.
57. Davis, E.E., Zhang, Q., Liu, Q., Diplas, B.H., Davey, L.M., Hartley, J., Stoetzel, C., Szymanska, K., Ramaswami, G., Logan, C.V. *et al.* (2011) TTC21B contributes both causal and modifying alleles across the ciliopathy spectrum. *Nat. Genet.*, **43**, 189–196.
58. Anderson, E., Peluso, S., Lettice, L.A. and Hill, R.E. (2012) Human limb abnormalities caused by disruption of hedgehog signaling. *Trends Genet.*, **28**, 364–373.
59. St-Jacques, B., Hammerschmidt, M. and McMahon, A.P. (1999) Indian hedgehog signaling regulates proliferation and differentiation of chondrocytes and is essential for bone formation. *Genes Dev.*, **13**, 2072–2086.
60. Haycraft, C.J. and Serra, R. (2008) Cilia involvement in patterning and maintenance of the skeleton. *Curr. Top. Dev. Biol.*, **85**, 303–332.
61. Vertii, A., Bright, A., Delaval, B., Hehnly, H. and Doxsey, S. (2015) New frontiers: discovering cilia-independent functions of cilia proteins. *EMBO Rep.*, **16**, 1275–1287.
62. Delaval, B., Bright, A., Lawson, N.D. and Doxsey, S. (2011) The cilia protein IFT88 is required for spindle orientation in mitosis. *Nat. Cell Biol.*, **13**, 461–468.
63. Pazour, G.J., Dickert, B.L., Vucica, Y., Seeley, E.S., Rosenbaum, J.L., Witman, G.B. and Cole, D.G. (2000) Chlamydomonas IFT88 and its mouse homologue, polycystic kidney disease gene tg737, are required for assembly of cilia and flagella. *J. Cell Biol.*, **151**, 709–718.
64. Graser, S., Stierhof, Y.D., Lavoie, S.B., Gassner, O.S., Lamla, S., Le Clech, M. and Nigg, E.A. (2007) Cep164, a novel centriole appendage protein required for primary cilium formation. *J. Cell Biol.*, **179**, 321–330.
65. Davis, E.E. and Katsanis, N. (2012) The ciliopathies: a transitional model into systems biology of human genetic disease. *Curr. Opin. Genet. Dev.*, **22**, 290–303.
66. Oh, E.C., Vasanth, S. and Katsanis, N. (2015) Metabolic regulation and energy homeostasis through the primary Cilium. *Cell Metab.*, **21**, 21–31.
67. Siljee, J.E., Wang, Y., Bernard, A.A., Ersoy, B.A., Zhang, S., Marley, A., von Zastrow, M., Reiter, J.F. and Vaisse, C. (2018) Subcellular localization of MC4R with ADCY3 at neuronal primary cilia underlies a common pathway for genetic predisposition to obesity. *Nat. Genet.*, **50**, 180–185.
68. Davenport, J.R., Watts, A.J., Roper, V.C., Croyle, M.J., van Groen, T., Wyss, J.M., Nagy, T.R., Kesterson, R.A. and Yoder, B.K. (2007) Disruption of intraflagellar transport in adult mice leads to obesity and slow-onset cystic kidney disease. *Curr. Biol.*, **17**, 1586–1594.
69. Stratigopoulos, G., Martin Carli, J.F., O'Day, D.R., Wang, L., Leduc, C.A., Lanzano, P., Chung, W.K., Rosenbaum, M., Egli, D., Doherty, D.A. *et al.* (2014) Hypomorphism for RPGRIP1L, a ciliary gene vicinal to the FTO locus, causes increased adiposity in mice. *Cell Metab.*, **19**, 767–779.
70. Saeed, S., Bonnefond, A., Tamanini, F., Mirza, M.U., Manzoor, J., Janjua, Q.M., Din, S.M., Gaitan, J., Milochau, A., Durand, E. *et al.* (2018) Loss-of-function mutations in ADCY3 cause monogenic severe obesity. *Nat. Genet.*, **50**, 175–179.
71. Grarup, N., Moltke, I., Andersen, M.K., Dalby, M., Vitting-Seerup, K., Kern, T., Mahendran, Y., Jorsboe, E., Larsen, C.V.L., Dahl-Petersen, I.K. *et al.* (2018) Loss-of-function variants in ADCY3 increase risk of obesity and type 2 diabetes. *Nat. Genet.*, **50**, 172–174.
72. Tang, Z., Lin, M.G., Stowe, T.R., Chen, S., Zhu, M., Stearns, T., Franco, B. and Zhong, Q. (2013) Autophagy promotes primary ciliogenesis by removing OFD1 from centriolar satellites. *Nature*, **502**, 254–257.
73. Schroder, J.M., Larsen, J., Komarova, Y., Akhmanova, A., Thorsteinsson, R.I., Grigoriev, I., Manguso, R., Christensen, S.T., Pedersen, S.F., Geimer, S. *et al.* (2011) EB1 and EB3 promote cilia biogenesis by several centrosome-related mechanisms. *J. Cell Sci.*, **124**, 2539–2551.
74. Schroder, J.M., Schneider, L., Christensen, S.T. and Pedersen, L.B. (2007) EB1 is required for primary cilia assembly in fibroblasts. *Curr. Biol.*, **17**, 1134–1139.
75. Dammermann, A. and Merdes, A. (2002) Assembly of centrosomal proteins and microtubule organization depends on PCM-1. *J. Cell Biol.*, **159**, 255–266.
76. Kim, J., Krishnaswami, S.R. and Gleeson, J.G. (2008) CEP290 interacts with the centriolar satellite component PCM-1 and is required for Rab8 localization to the primary cilium. *Hum. Mol. Genet.*, **17**, 3796–3805.

77. Silva, E., Betleja, E., John, E., Spear, P., Moresco, J.J., Zhang, S., Yates, J.R., 3rd, Mitchell, B.J. and Mahjoub, M.R. (2016) Ccdc11 is a novel centriolar satellite protein essential for ciliogenesis and establishment of left–right asymmetry. *Mol. Biol. Cell*, **27**, 48–63.
78. Singla, V., Romaguera-Ros, M., Garcia-Verdugo, J.M. and Reiter, J.F. (2010) Ofd1, a human disease gene, regulates the length and distal structure of centrioles. *Dev. Cell*, **18**, 410–424.
79. Ferrante, M.I., Zullo, A., Barra, A., Bimonte, S., Messaddeq, N., Studer, M., Dolle, P. and Franco, B. (2006) Oral-facial-digital type I protein is required for primary cilia formation and left–right axis specification. *Nat. Genet.*, **38**, 112–117.
80. Azimzadeh, J., Nacry, P., Christodoulidou, A., Drevensek, S., Camilleri, C., Amiour, N., Parcy, F., Pastuglia, M. and Bouchez, D. (2008) Arabidopsis TONNEAU1 proteins are essential for preprophase band formation and interact with centrin. *Plant Cell*, **20**, 2146–2159.
81. Church, G.M. and Gilbert, W. (1984) Genomic sequencing. *Proc. Natl. Acad. Sci. U. S. A.*, **81**, 1991–1995.